

Single Coil Multi-Slice Aliasing and Separation for FMRI

Daniel B. Rowe^{1,2} and Mary C. Kociuba¹

¹Department of Mathematics, Statistics and Computer Science, Marquette University

²Department of Biophysics, Medical College of Wisconsin

Abstract

In functional magnetic resonance imaging, images of the brain are acquired as rapidly as physically possible to cover the necessary brain, but also to capture cognitive temporal dynamics. Techniques for in-plane acceleration such as SENSE and GRAPPA have greatly contributed to decreasing image scan time. Newer simultaneous multi-slice (SMS) methods have taken a different approach by accelerating through-plane to decrease scan time. Two multi-slice aliasing techniques are examined for through-plane SMS acceleration.

Key Words: fMRI, parallel slice, multiband, image reconstruction, magnetic resonance imaging, CAIPI, Hadamard

1. Introduction

In functional magnetic resonance imaging (fMRI), an image volume is generally formed from slices of images. The measured data by the MRI machine for a slice are spatial frequencies (k -space). It generally takes up to two seconds to measure full arrays of data for all of the slices that form the volume image. A tremendous amount of work has been and is currently being devoted to accelerating the number images acquired per unit of time since its initial postulation (1). Significant advances in accelerating image acquisition have been made by subsampling k -space and skipping lines in-plane (IP). When lines of k -space are skipped, the reconstructed images are aliased. Two major approaches have been developed to unalias IP aliased images. The first SENSitivity Encoding (SENSE) operates on aliased images (2), while the second GeneRalized Autocalibrating Partial Parallel Acquisition (GRAPPA) operates on subsampled k -space (3). More recently, efforts have been aimed at applying IP techniques through-plane (TP). In TP also known as simultaneous multi-slice (SMS), several slices are simultaneously magnetized and the k -space data that is measured is the sum of the k -space data that would arise from each of the multiple slices (4-6). Most SMS techniques, rely upon multiple coils in order to separate multiply aliased slices. Recently the Separation of Parallel Encoded Complex-valued Slices (SPECS) model was introduced to separate two or more slices from a single channel coil (7,8). When the SPECS model was introduced, it utilized Controlled Aliasing in Parallel Imaging Results in Higher Acceleration (CAIPIRINHA) shifts to decrease the similarity between the overlapping slices. An alternative to decrease the similarity between overlapping slices is to use Hadamard sign encoding of the slices to be aliased. After CAIPIRINHA shift and Hadamard sign encoded images are separated, complex-valued images result, and hence complex-valued activation is computed (9-10). Here, CAIPIRINHA shift and Hadamard sign encodings along with their separations are examined within the SPECS SMS framework (11-12).

2. Background

In SMS MR imaging, a single slice image is measured that consists of the sum of the

true individual slice images plus additive measurement error. The goal of SMS image encoding and reconstruction is to measure one image, and from this one image separate two or more images. If the images that are aliased are too similar, then it is more challenging to separate them. Therefore, it is desirable to maximize the difference between the aliased images. The CAIPIRINHA approach that has been utilized with some success is to add magnetization to each slice so that they individually appear shifted in the field-of-view (FOV). Another approach that is gaining interest is to Hadamard encode the individual images, that is, add magnetization to or subtract it from each image before they are aliased. When these individual images are aliased, then the similar voxels are in different locations due to the shifting or have different signs due to Hadamard encoding.

2.1 CAIPI Shift Encoding

To illustrate and explain the CAIPIRINHA FOV shifting, consider an example where $N_S=4$ slices are aliased and a single slice image measured. With the four slices, each can be shifted within the FOV by either A: (0/4)FOV, B: (1/4)FOV, C: (2/4)FOV, or D: (3/4)FOV. With each of these $N_S=4$ possible shifts, there are $N_S=4$ basic patterns of shifting as illustrated in Figure 1 (neglecting measurement error). We can think of each of the patterns as blocks in a Latin square block design signified by the capital letter in the lower right area in the individual images. At any given time point, one of these patterns of aliasing can be selected and measured.

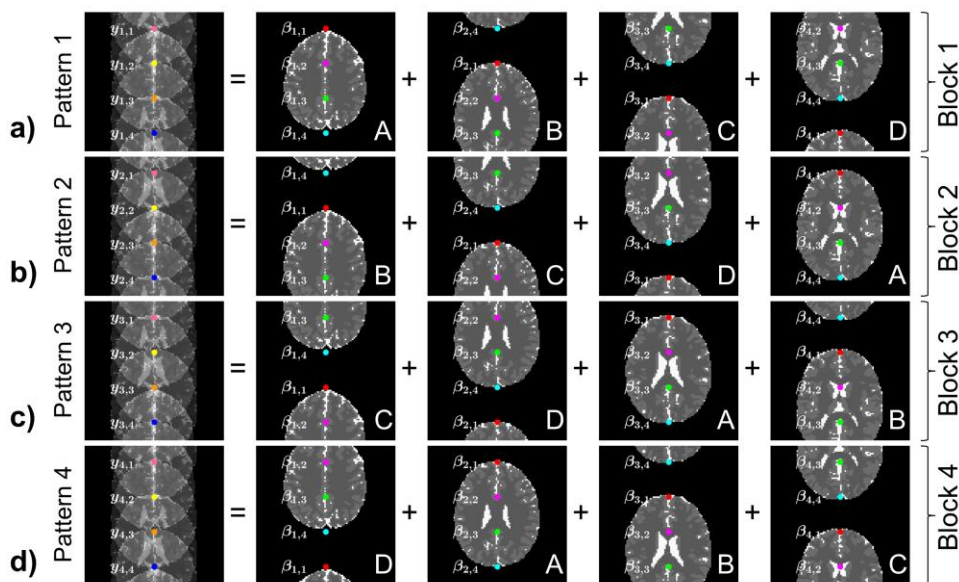


Figure 1. CAIPIRINHA shifted images in aliasing process.

The goal of SMS is to get more than one image per unit time. We can obtain $N_S=4$ slices in one time measurement (pattern 1 in Figure 1a) then separate them for an acceleration factor of $A=4$, or obtain $N_S=4$ slices in $N_{acq}=2$ time measurements (patterns 1 and 2 in Figures 1a and 1b) then separate them for an acceleration factor of $A=2$, or obtain $N_S=4$ slices in $N_{acq}=3$ time measurements then separate them for an acceleration factor of $A=4/3$. Obtaining $N_S=4$ slices in $N_{acq}=4$ time measurements then separating yields an acceleration factor of $A=1$, which is no increase in image acquisition.

In Figure 1, denote the observed aliased voxel value at time image t in voxel location ℓ

as $y_{t,\ell}$ and the true voxel value in slice j in voxel location ℓ as $\beta_{j\ell}$. If we examine shift pattern 1 in Figure 1a, we can see that we have measurements at time $t=1$ in location $\ell=1$ that is $y_{1,1} = \beta_{1,1} + \beta_{2,4} + \beta_{3,3} + \beta_{4,2}$, in location 2 that is $y_{1,2} = \beta_{1,2} + \beta_{2,1} + \beta_{3,4} + \beta_{4,3}$, that is $y_{1,3} = \beta_{1,3} + \beta_{2,2} + \beta_{3,1} + \beta_{4,4}$, that is $y_{1,4} = \beta_{1,4} + \beta_{2,3} + \beta_{3,2} + \beta_{4,1}$. Similarly, upon examining shift pattern 2 we have $y_{2,1} = \beta_{1,4} + \beta_{2,3} + \beta_{3,2} + \beta_{4,1}$, in location 2 that is $y_{2,2} = \beta_{1,1} + \beta_{2,4} + \beta_{3,3} + \beta_{4,2}$, that is $y_{2,3} = \beta_{1,2} + \beta_{2,1} + \beta_{3,4} + \beta_{4,3}$, that is $y_{2,4} = \beta_{1,3} + \beta_{2,2} + \beta_{3,1} + \beta_{4,4}$. We can gather the measured values at the $N_S N_{acq} = 8$ locations in the $N_{acq} = 2$ images in vector form in terms of the true values as

$$\begin{bmatrix} y_{1,1} \\ y_{1,2} \\ y_{1,3} \\ y_{1,4} \\ y_{2,1} \\ y_{2,2} \\ y_{2,3} \\ y_{2,4} \end{bmatrix} = \begin{bmatrix} 1 & 0 & 0 & 0 & 0 & 0 & 0 & 1 & 0 & 0 & 1 & 0 & 0 & 1 & 0 & 0 \\ 0 & 1 & 0 & 0 & 1 & 0 & 0 & 0 & 0 & 0 & 1 & 0 & 0 & 1 & 0 & 0 \\ 0 & 0 & 1 & 0 & 0 & 1 & 0 & 0 & 1 & 0 & 0 & 0 & 0 & 0 & 0 & 1 \\ 0 & 0 & 0 & 1 & 0 & 0 & 1 & 0 & 0 & 1 & 0 & 0 & 1 & 0 & 0 & 0 \\ 0 & 0 & 0 & 1 & 0 & 0 & 1 & 0 & 0 & 1 & 0 & 0 & 1 & 0 & 0 & 0 \\ 1 & 0 & 0 & 0 & 0 & 0 & 0 & 1 & 0 & 0 & 1 & 0 & 0 & 1 & 0 & 0 \\ 0 & 1 & 0 & 0 & 1 & 0 & 0 & 0 & 0 & 0 & 1 & 0 & 0 & 1 & 0 & 0 \\ 0 & 0 & 1 & 0 & 0 & 1 & 0 & 0 & 1 & 0 & 0 & 0 & 0 & 0 & 0 & 1 \end{bmatrix} \cdot \begin{bmatrix} \beta_{1,1} \\ \beta_{1,2} \\ \beta_{1,3} \\ \beta_{1,4} \\ \beta_{2,1} \\ \beta_{2,2} \\ \beta_{2,3} \\ \beta_{2,4} \\ \beta_{3,1} \\ \beta_{3,2} \\ \beta_{3,3} \\ \beta_{3,4} \\ \beta_{4,1} \\ \beta_{4,2} \\ \beta_{4,3} \\ \beta_{4,4} \end{bmatrix} \quad [1]$$

In Equation 1, we can see that we have a system of $N_S N_{acq} = 8$ equations with sixteen unknowns. If we includes all $N_S = 4$ patterns or blocks in Equation 1 then we would have $N_S^2 = 16$ equations and $N_S^2 = 16$ unknowns, but no image acceleration. An acceleration of $A = 2$ will be utilized to compare CAIPIRINHA shift to Hadamard sign encoding, thus making this a fractional block design. Equation 1 for CAIPIRINHA shift encodings can be written as $y_C = X_C \beta + \epsilon_C$, where measurement error has been included. The SPECS model will be described in Section 3 to remedy the underdetermined system so that the aliased images can be properly separated.

2.2 Hadamard Sign Encoding

Similar to the aliased images via CAIPIRINHA shifts, images can be aliased with Hadamard sign encoding. To illustrate and explain the Hadamard encoding, consider an example where $N_S = 4$ slices are aliased and a single slice image measured. With the $N_S = 4$ slices, each can be assigned a sign of “+” or “-” before aliasing. With the sign assignment, there are $N_S = 4$ possible ways that we can produce orthogonal linear combinations as illustrated in Figure 2 (neglecting measurement error). We can think of each of the patterns as orthogonal contrasts or blocks in an experimental design. At any given time point, one of these patterns of aliasing can be selected and measured.

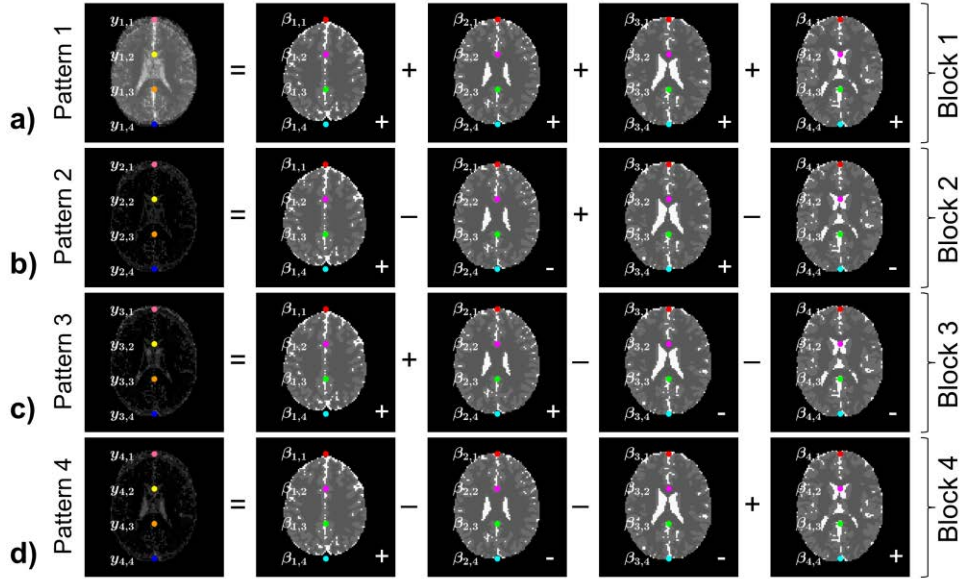


Figure 2. Hadamard sign encoded images in aliasing process.

As with the CAIPIRINHA shifting, the goal with Hadamard encoding is to get more than one image per unit time. We can obtain $N_S=4$ slices in $N_{acq}=1$ time measurement (pattern 1 in Figure 2a) then separate them for an acceleration factor of $A=4$, or obtain $N_S=4$ slices in $N_{acq}=2$ time measurements (patterns 1 and 2 in Figures 2a and 2b) then separate them for an acceleration factor of $A=2$, or obtain $N_S=4$ slices in $N_{acq}=3$ time measurements then separate them for an acceleration factor of $A=4/3$. Obtaining $N_S=4$ slices in $N_{acq}=4$ time measurements then separating yields an acceleration factor of $A=1$, which is again no increase in image acquisition.

In Figure 2, denote the observed aliased voxel value at time image t in voxel location l as $y_{t,l}$ and the true voxel value in slice j in voxel location l as $\beta_{j,l}$. If we examine shift pattern 1 in Figure 2a, we can see that we have measurements at time $t=1$ in location $l=1$ that is $y_{1,1} = \beta_{1,1} + \beta_{2,1} + \beta_{3,1} + \beta_{4,1}$, in location 2 that is $y_{1,2} = \beta_{1,2} + \beta_{2,2} + \beta_{3,2} + \beta_{4,2}$, that is $y_{1,3} = \beta_{1,3} + \beta_{2,3} + \beta_{3,3} + \beta_{4,3}$, that is $y_{1,4} = \beta_{1,4} + \beta_{2,4} + \beta_{3,4} + \beta_{4,4}$. Similarly, upon examining shift pattern 2 we have $y_{2,1} = \beta_{1,1} - \beta_{2,1} + \beta_{3,1} - \beta_{4,1}$, in location 2 that is $y_{2,2} = \beta_{1,1} - \beta_{2,1} + \beta_{3,1} - \beta_{4,1}$, that is $y_{2,3} = \beta_{1,3} - \beta_{2,3} + \beta_{3,3} - \beta_{4,3}$, that is $y_{2,4} = \beta_{1,4} - \beta_{2,4} + \beta_{3,4} - \beta_{4,4}$. We can gather the measured values at the $N_S N_{acq} = 8$ locations in the $N_{acq} = 2$ images in vector form in terms of the true values as

$$\begin{bmatrix} y_{1,1} \\ y_{1,2} \\ y_{1,3} \\ y_{1,4} \\ y_{2,1} \\ y_{2,2} \\ y_{2,3} \\ y_{2,4} \end{bmatrix} = \begin{bmatrix} 1 & 0 & 0 & 0 & 1 & 0 & 0 & 0 & 1 & 0 & 0 & 0 & 1 & 0 & 0 & 0 \\ 0 & 1 & 0 & 0 & 0 & 1 & 0 & 0 & 0 & 1 & 0 & 0 & 0 & 1 & 0 & 0 \\ 0 & 0 & 1 & 0 & 0 & 0 & 1 & 0 & 0 & 0 & 1 & 0 & 0 & 0 & 1 & 0 \\ 0 & 0 & 0 & 1 & 0 & 0 & 0 & 1 & 0 & 0 & 0 & 1 & 0 & 0 & 0 & 1 \\ 1 & 0 & 0 & 0 & -1 & 0 & 0 & 0 & 1 & 0 & 0 & 0 & -1 & 0 & 0 & 0 \\ 0 & 1 & 0 & 0 & 0 & -1 & 0 & 0 & 0 & 1 & 0 & 0 & 0 & -1 & 0 & 0 \\ 0 & 0 & 1 & 0 & 0 & 0 & -1 & 0 & 0 & 0 & 1 & 0 & 0 & 0 & -1 & 0 \\ 0 & 0 & 0 & 1 & 0 & 0 & 0 & -1 & 0 & 0 & 0 & 1 & 0 & 0 & 0 & -1 \end{bmatrix} \cdot \begin{bmatrix} \beta_{1,1} \\ \beta_{1,2} \\ \beta_{1,3} \\ \beta_{1,4} \\ \beta_{2,1} \\ \beta_{2,2} \\ \beta_{2,3} \\ \beta_{2,4} \\ \beta_{3,1} \\ \beta_{3,2} \\ \beta_{3,3} \\ \beta_{3,4} \\ \beta_{4,1} \\ \beta_{4,2} \\ \beta_{4,3} \\ \beta_{4,4} \end{bmatrix} \quad [2]$$

Similar to Equation 1, in Equation 2 we can see that we have a system of $N_S N_{acq}=8$ equations with $N_S^2=16$ unknowns. If we includes all $N_S=4$ patterns or blocks in Equation 2 then we would have $N_S^2=16$ equations and $N_S^2=16$ unknowns, but no image acceleration. An acceleration of $A=2$ will be utilized to compare CAIPIRINHA shift to Hadamard sign encoding, thus making this a fractional block design. Equation 2 for Hadamard sign encodings can be written as $y_H=X_H\beta+\varepsilon_H$, where measurement error has been included. As previously noted, the SPECS model will be described in Section 3 to remedy the underdetermined system so that the aliased images can be properly separated.

3. Methods

Since we can't separate the images solely based upon the data that we have from the experiment as in Equations 1 and 2, we need additional information. One way to obtain additional image information is to acquire complete nonaliased calibration images of the slices within each aliased image and utilize these for image separation. The process to separate the aliased images is similar for both CAIPIRINHA shift and Hadamard sign aliased images.

In order to increase identifiability in Equations 1 and 2 that have eight equations and sixteen unknowns, additional rows are added as measured data, as design matrix rows, and as measurement error. Let $y_A = y_C$ or y_H be the measured aliased image data, $X_A = X_C$ or X_H be, the aliasing design matrix, and $\varepsilon_A = \varepsilon_C$ or ε_H be the additive measurement error. The goal of the SPECS model (7,8) is to add additional image information to obtain identifiability. The previous illustrative description of the CAIPIRINHA shift and Hadamard sign encoding processes needs to be utilized for each of the real and imaginary parts of the complex-valued data. The additional information needed in order to obtain identifiability in Equations 1 and 2 is obtained from full nonaliased prior calibration images of the same slices to be aliased.

Consider a time series of length m fully sampled calibration images for the $N_S=4$ slices. At time point t , a single voxel in slice z , $z = 1, \dots, N_S=4$ of the calibration images is denoted by $v_{z,t}=(\mu_{Rz}+i\mu_{Iz})+(\eta_{Rz,t}+i\eta_{Iz,t})$, where μ_{Rz} and μ_{Iz} , are the true real and imaginary components. While $\eta_{Rz,t}$ and $\eta_{Iz,t}$ denote the real and imaginary components of the measurement error, with a mean of $E(\eta_{Rt}^T, \eta_{It}^T)^T=0$ and a covariance of

$\text{cov}(\eta_{Ri}^T, \eta_{Ii}^T)^T = \sigma^2 I_{N_S}$. The mean of the m calibration images for a voxel values in the same location across N_S slices is written into a single real-valued vector that is the concatenation of each of the real and imaginary vectors as

$$\begin{pmatrix} \bar{v}_R \\ \bar{v}_I \end{pmatrix} = (\bar{v}_{R,1}, \dots, \bar{v}_{R,N_S}, \bar{v}_{I,1}, \dots, \bar{v}_{I,N_S})^T, \quad [3]$$

where \bar{v}_R and \bar{v}_I denote $N_S \times 1$ vectors with the mean real and imaginary component of the N_S voxel values. The mean calibration vectors \bar{v} are incorporated into the SPECS model with an artificial Hadamard aliasing scheme.

The aliasing process outlined in Equations 1 and 2 represents an underdetermined system of $N_{acq}N_S = 8$ equations and $N_S^2 = 16$ unknowns. To make the system of equations in Equations 1 and 2 solvable, at least $(N_S - N_{acq})N_S = 8$ rows need to be added to both X_A and y_A in order to increase the rank to $N_S^2 = 16$. The SPECS approach for $N_S = 4$ aliased slices first constructs an $(N_S - N_{acq}) \times N_S$ artificial aliasing matrix C , consisting of the remaining $(N_S - N_{acq})$ orthogonal Hadamard ways (aliasing patterns) the true voxel values in the N_S slices could be aliased. Then the coefficients C are incorporated into the model by denoting the block of N_S columns in X_A that correspond to slice j by X_{Aj} , the j^{th} column of the matrix C by C_j , and forming the artificial aliasing matrix, $C_A = [X_1 \otimes C_1, \dots, X_{N_S} \otimes C_{N_S}]$. To complete the SPECS model, the vectors \bar{v}_R and \bar{v}_I are not the average of all m calibration images, but when separating each N_{acq} patterns, a random sample of $N_S N_{acq}$ calibration images is selected to be retrospectively averaged and Hadamard sign encoded.

Both observed aliased voxel values y_{AR} and y_{AI} along with the artificially aliased mean voxel values \bar{v}_R and \bar{v}_I are combined and represented by

$$y = \begin{pmatrix} y_{AR} \\ C_A \bar{v}_R \\ y_{AI} \\ C_A \bar{v}_I \end{pmatrix} = \begin{pmatrix} X_A \beta_R \\ C_a \mu_R \\ X_A \beta_I \\ C_A \mu_I \end{pmatrix} + \begin{pmatrix} \varepsilon_R \\ C_A \eta_R \\ \varepsilon_I \\ C_A \eta_I \end{pmatrix}. \quad [4]$$

In Equation 4, the added error vector consists of the measurement error of the observed aliased voxels ε_R and ε_I along with the measurement error of the artificially aliased mean of sampled calibration images $C_A \eta_R$ and $C_A \eta_I$. It can be seen that the images can be separated with a least squares estimator for the true images in the usual way as

$$\hat{\beta} = (X'X)^{-1} X'y, \quad [5]$$

where $X = [X_A; C_A]$ and y is as defined in Equation 4. Taking a closer look at the separated images in Equation 5, the mean vector and covariance matrix can be determined. With a little algebra, the expected value and the covariance matrix for $\hat{\beta}$ can be determined to be

$$E(\hat{\beta}) = \beta \quad [6]$$

and

$$\text{cov}(\hat{\beta}) = \frac{\sigma^2}{N_S N_{acq}} \quad [7]$$

for both encoding schemes. The mean of the separated images is the true image values and the separated images are uncorrelated with appropriately reduced variance. These are very desirable properties for the separated images. Correlated images, referred to as signal leakage, is a pervasive problem in SMS fMRI.

4. Results

To evaluate and compare the CAIPIRINHA shift and Hadamard sign image encoding schemes, simulated data is generated. A T_2^* weighted 96×96 digital phantom is generated with 720 TRs for $N_S=4$ slices. For the optimal separation, a unique magnitude and phase is included in each slice, with an average signal-to-noise ratio (SNR), mean divided by standard deviation of $\text{SNR} = 50$, and with a contrast-to-noise ratio (CNR) of $1/2$. One voxel region in each slice, with the locations rotating clockwise, has a block design task simulated consisting of 16 seconds of non-task followed by 22 replications of 16 seconds of task then 16 seconds of non-task. The block design task was added to its magnitude with a contrast to noise ratio (CNR), task amplitude of $\text{CNR} = 1/2$. In both models the initial $m=16$ non-task portion of the time-series is used for the calibration images in the slice separation and the remaining $n=704$ images separated.

4.1 CAIPIRINHA Shift Encoding

The image separation process in Equation 5 with measured CAIPIRINHA shift aliased images as described in Equation 1 was applied to the simulated data. Results for an acceleration factor $A=2$ are presented in Figure 3. The magnitude of the mean separated

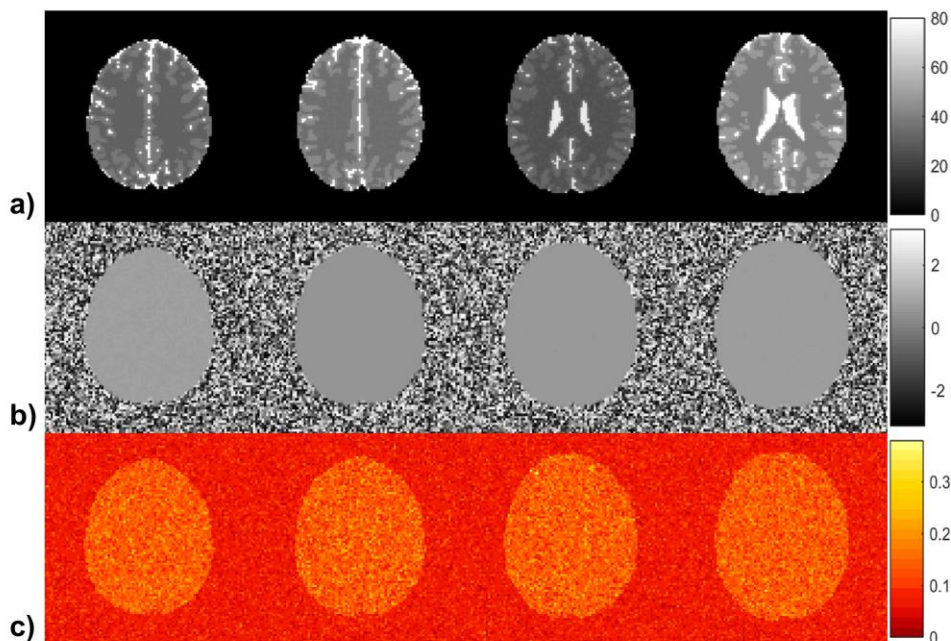


Figure 3. Results for CAIPIRINHA shift encoding separation. a) Magnitude of mean, b) Phase of mean, and c) Variance.

images are presented in Figure 3a and the phase of the mean image are in Figure 3b. Although not shown, there is no visual difference between the true magnitude and phase image values and the magnitude and phase of mean images in Figures 3a and 3b. The variances of the separated images are presented in Figure 3c.

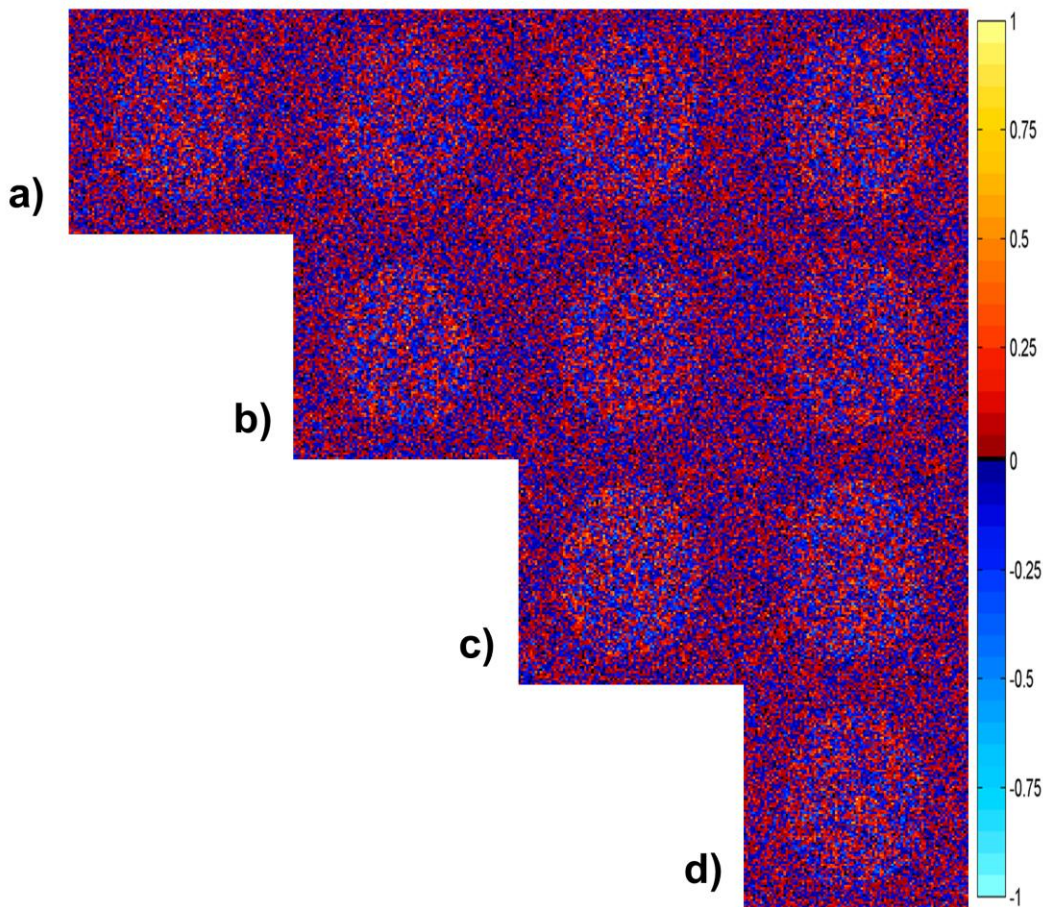


Figure 4. Results for CAIPIRINHA shift encoding separation. a) Magnitude square correlation between center voxel in slice 1 and voxels in other slices, b) Magnitude square correlation between center voxel in slice 2 and voxels in slices 2-4, c) Magnitude square correlation between center voxel in slice 3 and voxels in slices 3-4, d) Magnitude square correlation between center voxel in slice 4 and voxels in slice 4.

One of the main issues with SMS encoding and separation is that there is often correlation between the voxels in the separated slices for the same (x,y) location. The magnitude square correlation from the complex-valued separated images is presented in Figure 4. In Figure 4a are the correlations between the center voxel in slice 1 and the others in slice 1 through slice 4. In Figure 4b are the correlations between the center voxel in slice 2 and the others in slice 2 through slice 4. In Figure 4c are the correlations between the center voxel in slice 3 and the others in slice 3 and slice 4. In Figure 4d are the correlations between the center voxel in slice 4 and the others in slice 4. What can be seen in Figure 4 is that there is no significant correlation between the separated slices.

Since the separated images are complex-valued, complex-valued fMRI activation was computed (9). The results for $A=1$ are presented in Figure 5a, for $A=2$ in Figure 5b, and for $A=4$ in Figure 5c. The activation for $A=2$ in Figure 5b appears similar to the activation for $A=1$ in Figure 5a. The activation for $A=4$ appears to have signal leakage between the slices, meaning that the activation is not placed in the correct slice.

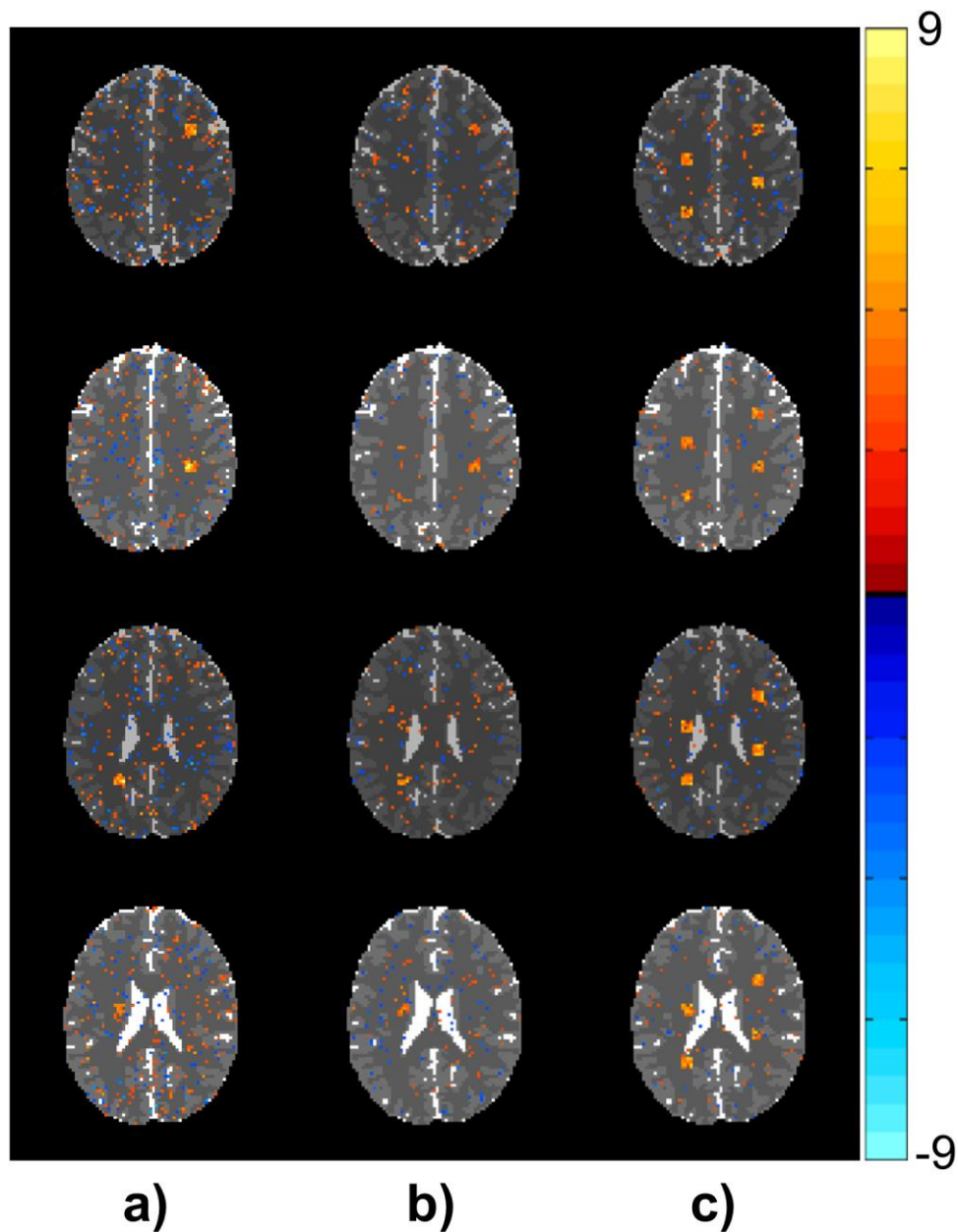


Figure 5. Complex-valued activation from CAIPRINHA shift separated images. a) Acceleration $A=1$, b) Acceleration $A=2$, c) Acceleration $A=4$.

4.2 Hadamard Sign Encoding

The image separation process in Equation 5 with measured Hadamard sign aliased images as described in Equation 2 was applied to the simulated data. Results for an acceleration factor $A=2$ are presented in Figure 6. The magnitude of the mean separated images are presented in Figure 6a and the phase of the mean image are in Figure 6b. Although not shown, there is a small visual difference between the true magnitude and phase image values and the magnitude and phase of mean images in Figure 6a and 6b. The means of the separated images for the Hadamard sign encoding is slightly darker. The variance of the separated images are presented in Figure 6c.

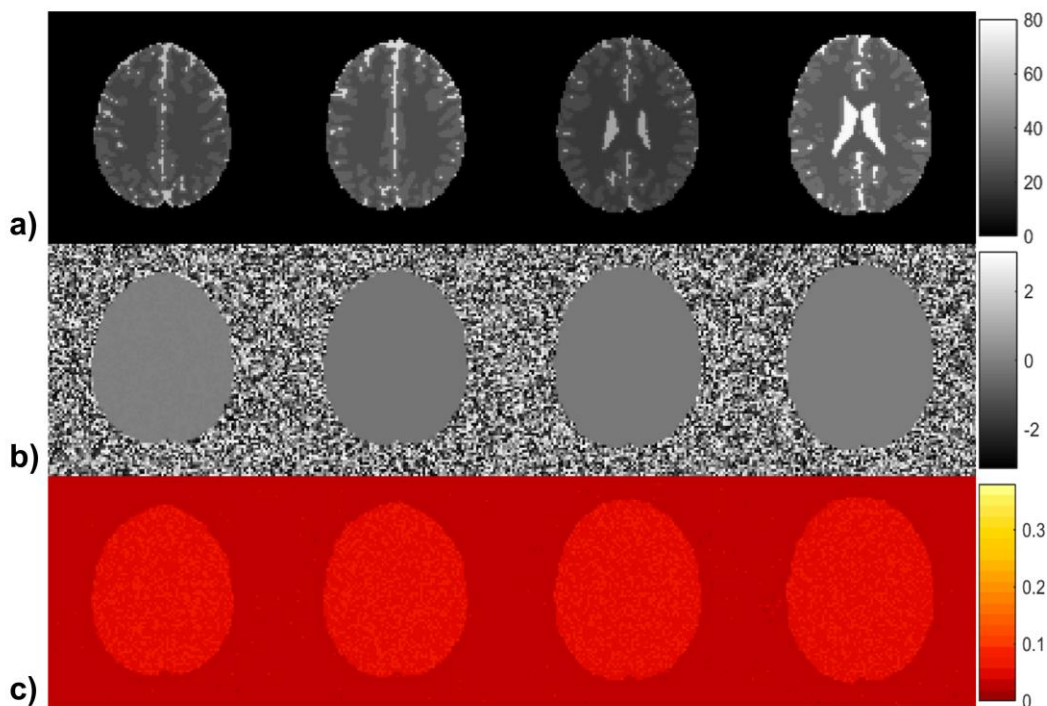


Figure 6. Results for Hadamard sign encoding separation. a) Magnitude of mean, b) Phase of mean, and c) Variance.

As previously noted, one of the main issues with SMS encoding and separation is that there is often correlation between the voxels in the separated slices for the same (x,y) location. The magnitude square correlation from the complex-valued separated images is presented in Figure 7. In Figure 7a are the correlations between the center voxel in slice 1 and the others in slice 1 through slice 4. In Figure 7b are the correlations between the center voxel in slice 2 and the others in slice 2 through slice 4. In Figure 7c are the correlations between the center voxel in slice 3 and the others in slice 3 and slice 4. In Figure 7d are the correlations between the center voxel in slice 4 and the others in slice 4. What can be seen in Figure 7 is that there is no significant correlation between the separated slices.

Since the separated images are complex-valued, complex-valued fMRI activation was computed (9). The results for $A=1$ are presented in Figure 8a, for $A=2$ in Figure 8b, and for $A=4$ in Figure 8c. The activation for $A=2$ in Figure 8b appears similar to the activation for $A=1$ in Figure 8a. The activation for $A=1$, 2, and 4 appears very similar and all extremely good with no signal leakage between the slices unlike what was seen with the CAIPRINHA shift aliased images.

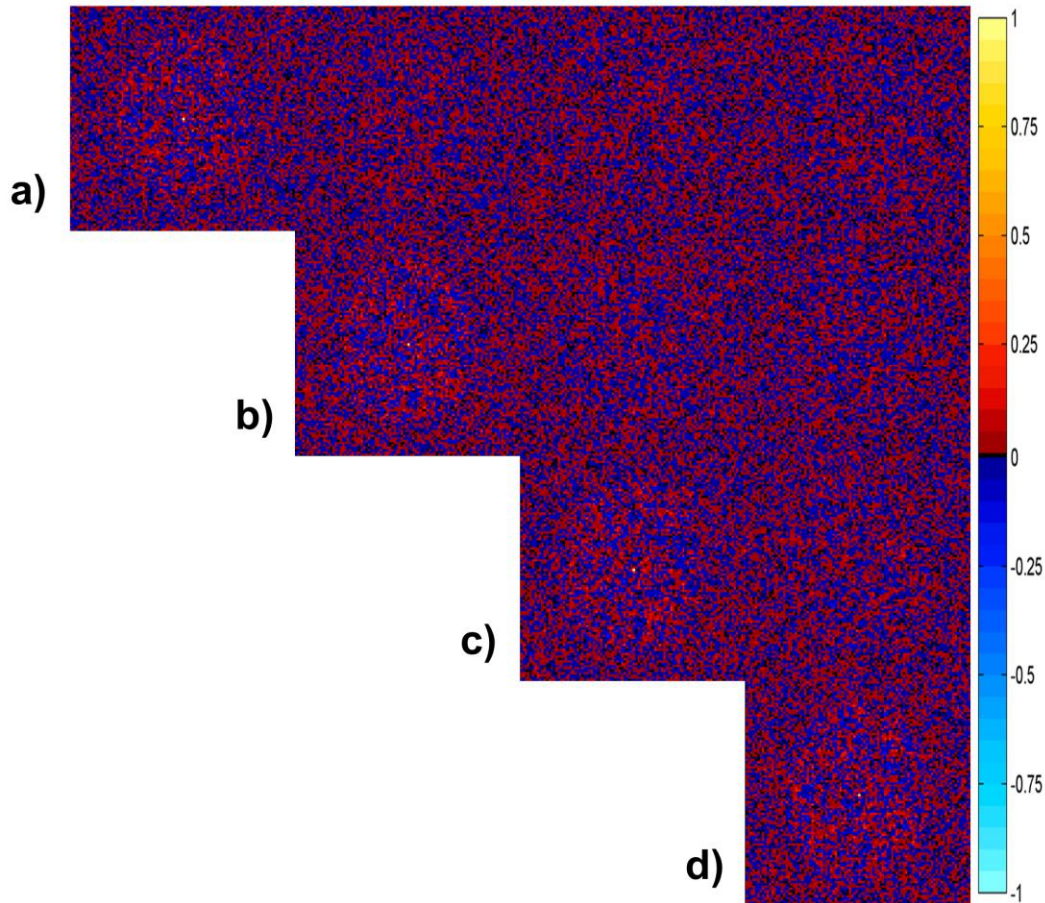


Figure 7. Results for Hadamard sign encoding separation. a) Magnitude square correlation between center voxel in slice 1 and voxels in other slices, b) Magnitude square correlation between center voxel in slice 2 and voxels in slices 2-4, c) Magnitude square correlation between center voxel in slice 3 and voxels in slices 3-4, d) Magnitude square correlation between center voxel in slice 4 and voxels in slice 4.

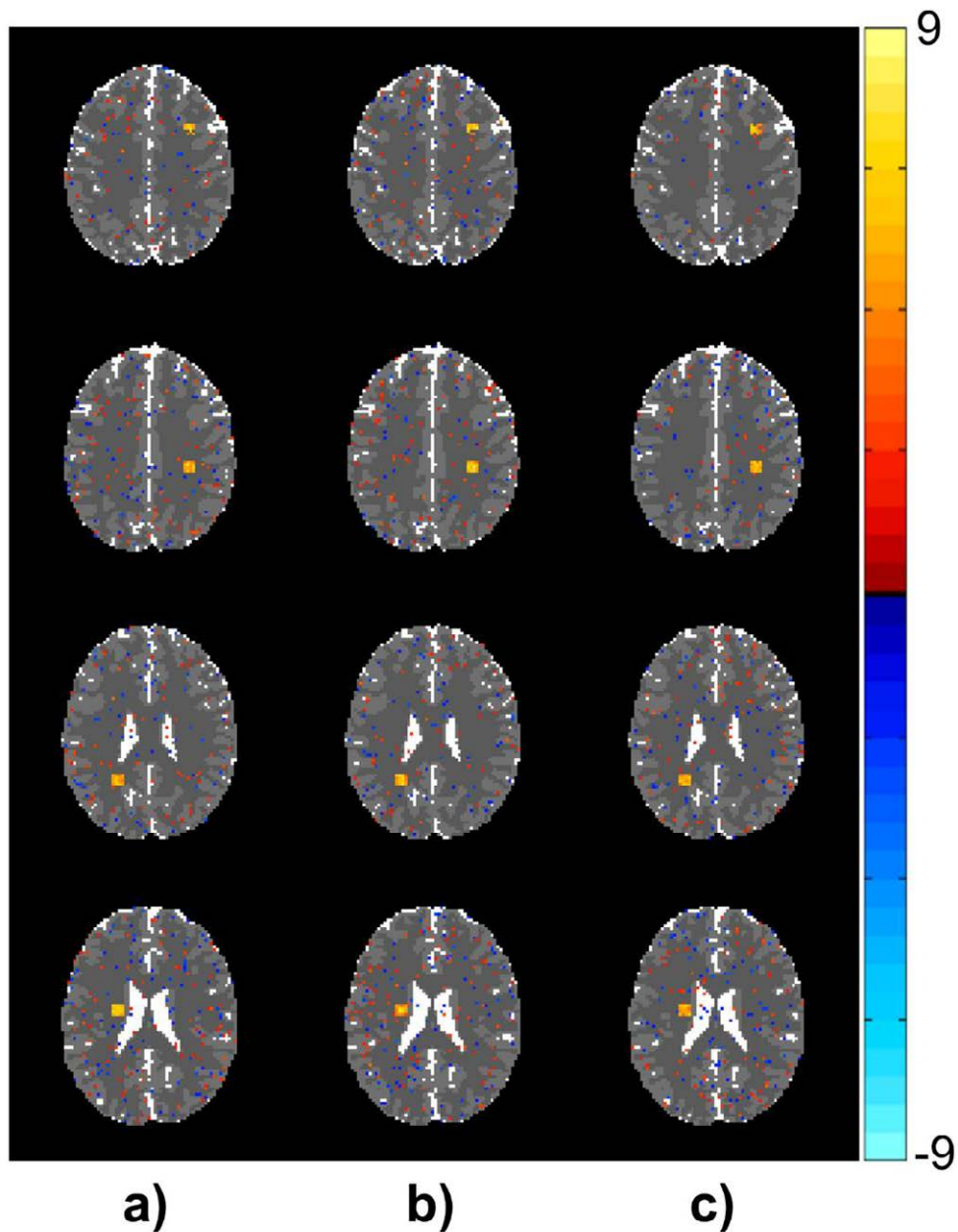


Figure 8. Complex-valued activation from Hadamard sign separated images. a) Acceleration $A=1$, b) Acceleration $A=2$, c) Acceleration $A=4$.

5. Discussion and Conclusions

It was theoretically demonstrated that the SPECS model separates CAIPRINHA shift and Hadamard sign encoded aliased images with the same mean and diagonal covariance matrix. However, simulation results indicate that the separated images after CAIPRINHA shift aliasing as compared to Hadamard sign aliasing produces better mean images, higher variance in the separated images, and higher through slice correlation. Also the simulation results indicate that the separated images after Hadamard sign aliasing as compared to CAIPRINHA shift aliasing produces mean images that are biased darker,

lower variance in the separated images, and negligible through slice correlation. These results are somewhat counter to the theoretical properties in Equations 6 and 7. According to Equations 6, we would expect the mean images from both types of aliased images to be the same and not statistically different from the true values, which they are not. Further, according to Equation 7, we would expect the variances from the two aliasing techniques to be the same and equal to $1/(N_s N_{acq})$, which they are not. Finally, we would also expect according to Equation 7 that the correlation between the separated slices would be the same for both aliasing methods would be the same and negligible, but it is not. It is possible that there was some subtlety overlooked when deriving the results in Equations 6 and 7 or that there was something overlooked when performing the simulation.

Since experimentally it is difficult to reconstruct a CAIPIRINHA aliased image due to an imperfect Nyquist ghost correction and not a Hadamard aliased image, and because in this simulation the Hadamard aliased images did not yield correlation between the slices, we recommend that Hadamard encoding be utilized for SMS aliasing.

Acknowledgements

This work was supported by National Institutes of Health research grant R21NS087450.

References

1. Hyde JS, Jesmanowicz A, Francisz W, Kneeland JB, Grist TM, Campagna NF Parallel image acquisition from noninteracting local coils. *J Magn Reson*, 70:512–517, 1986.
2. Pruessmann KP, Weiger M, Scheidegger MB, Boesiger P. SENSE: Sensitivity Encoding for Fast MRI. *Magn Reson Med*, 42:952–962, 1999.
3. Griswold MA, Jakob PM, Heidemann RM, Nittka M, Jellus V, Wang J, Kiefer B, Haase A. Generalized autocalibrating partially parallel acquisition (GRAPPA). *Magn Reson Med*, 47:1202–1210, 2002.
4. Muller S. Multifrequency selective RF pulses for multislice MR imaging. *Magn Reson Med*, 6:364–371, 1988.
5. Souza SP, Szumowski J, Dumoulin CL, Plewes DP, Glover G. SIMA: simultaneous multislice acquisition of MR images by Hadamard-encoded excitation. *J Comput Assist Tomogr*, 12:1026–1030, 1988.
6. Moeller S, Auerbach E, van de Moortele P-F, Adriany G, Ugurbil K. Functional MRI with 16-fold reduction using multibanded, multisite sampling. *Proc Intl Soc Magn Reson Med*, 16:2366, 2008.
7. Rowe DB, Hyde JS, Jesmanowicz A, Nencka AS: Separation of two simultaneously encoded slices with a single coil. *Proc Intl Soc Magn Reson Med*, 20:123, 2013.
8. Rowe DB, Bruce IP, Nencka AS, Hyde JS, Kociuba MC: Separation of Parallel Encoded Complex-valued Slices (SPECS) from a Single Complex-valued Aliased Image. *Magn Reson Imaging*, Conditionally Accepted, 2015.
9. Rowe DB, Logan BR. A complex way to compute fMRI activation. *Neuroimage*, 23:1078–92, 2004.
10. Rowe DB. Modeling both the magnitude and phase of complex-valued fMRI data. *Neuroimage*, 25(4):1310–24, 2005.
11. Rowe DB, Nencka AS: Statistical image reconstruction of two simultaneously excited fMRI slices, *Proc Joint Stat Meet*, 17:201–216, 2012.
12. Rowe DB, Hyde JS, Jesmanowicz A, Nencka AS: Separation of two simultaneously encoded slices with a single coil. *Proc Intl Soc Magn Reson Med*, 20:123, 2013.